SCIENCE CHINA
Chemistry

•ARTICLES•

January 2023 Vol.66 No.1: 259–265
https://doi.org/10.1007/s11426-022-1460-7

Converting CO_2 to ethanol on Ag nanowires with high selectivity investigated by *operando* Raman spectroscopy

Qiong Liu[1†], Xia-Guang Zhang[3†], Zi-Yu Du[2†], Can-Jun Zou[1], Huan-Yu Chen[1], Yu Zhao[2], Jin-Chao Dong[2], Ping-Ping Fang[1*] & Jian-Feng Li[2*]

[1]*MOE Key Laboratory of Bioinorganic and Synthetic Chemistry, The Key Lab of Low-carbon Chem & Energy Conservation of Guangdong Province, School of Chemistry, Sun Yat-sen University, Guangzhou 510275, China;*
[2]*State Key Laboratory of Physical Chemistry of Solid Surfaces, iChEM, College of Chemistry and Chemical Engineering, Xiamen University, Xiamen 361005, China;*
[3]*Key Laboratory of Green Chemical Media and Reactions, Ministry of Education, Collaborative Innovation Center of Henan Province for Green Manufacturing of Fine Chemicals, State Key College of Chemistry and Chemical Engineering, Henan Normal University, Xinxiang 453007, China*

Received July 31, 2022; accepted November 16, 2022; published online December 1, 2022

Electrochemical conversion of CO_2 into liquid fuels provides an efficient way to store the renewable energy in the production of fuels and chemicals. However, effectively converting CO_2 to ethanol remains extremely challenging due to the low activity and selectivity. Herein, we achieve a high ethanol Faradaic efficiency (FE) as high as 85% on Ag nanowires (NWs) for CO_2 electroreduction at −0.95 V. X-ray photoelectron spectroscopy and electrochemical experiments prove that such Ag NWs are partially oxidized. *Operando* Raman spectroscopy finds the important CO intermediate adsorbed on partially oxidized Ag NWs, facilitating the ethanol formation. Density functional theory calculations prove that the reaction energy of CO coupling with the *CHO to *COCHO intermediate on the partially oxidized Ag NWs is smaller than that on the surface of Cu, which explains why the ethanol FE of such partially oxidized Ag NWs can exceed that of Cu, and therefore is the most favorable pathway for the formation of C_2 products on partially oxidized Ag NWs. This study provides a new insight to design efficient catalysts and investigate the mechanisms to improve the selectivity.

surface-enhanced Raman spectroscopy, CO_2 electroreduction, electrocatalysis, *operando* spectroscopy, ethanol

Citation: Liu Q, Zhang XG, Du ZY, Zou CJ, Chen HY, Zhao Y, Dong JC, Fang PP, Li JF. Converting CO_2 to ethanol on Ag nanowires with high selectivity investigated by *operando* Raman spectroscopy. *Sci China Chem*, 2023, 66: 259–265, https://doi.org/10.1007/s11426-022-1460-7

1 Introduction

CO_2 electroreduction to valuable fuels and chemicals provides a promising avenue towards the storage of renewable electricity [1,2]. Researchers have focused on developing efficient catalysts to convert CO_2 into various useful products, which can not only convert intermittent renewable electricity into energy-dense fuels but also decrease the level of atmospheric CO_2 [3–5]. Among the various products, C_2 liquid products are a kind of promising fuels for the energy storage because they have high energy density and are easy to store [6]. However, electrochemical conversion of CO_2 to ethanol need high energy barrier because of the C–C coupling, as well as multiple proton and electron transfers that involve multiple intermediates [7,8]. Therefore, converting CO_2 to C_2 products, especially ethanol, is still difficult, making the development of efficient electrocatalysts and mechanism studies a great challenge.

†These authors contributed equally to this work.
*Corresponding authors (email: fangpp3@mail.sysu.edu.cn; li@xmu.edu.cn)

In order to obtain efficient electrocatalysts for CO_2 electroreduction, various nanostructures and techniques have been developed. Thus far, copper-based catalysts are the leading materials to produce multi-carbon products toward CO_2 electroreduction, especially for making C_2 products [9]. However, the copper-based electrocatalysts for making such C_2 products are still lack of selectivity, especially for ethanol [10,11]. Ag-based catalysts have exhibited high selectivity for CO_2 electroreduction to CO at low overpotentials with depressed H_2 evolution [12,13], but has been rarely reported to convert CO_2 to ethanol. CO is an important intermediate for C–C coupling [14]. Therefore, Ag has the potential to exhibit the high selectivity for C_2 products by tuning the adsorption energy of CO. Recently, our group have made great progress in obtaining ethanol with high Faradaic efficiency (FE) of 55% by sulfurized Ag through the intermediate of CO [15]. However, it is difficult for Ag alone to obtain high ethanol selectivity. Interestingly, partially oxidized Cu can greatly alter the adsorption and reaction energy of CO to improve the selectivity for CO_2 electroreduction [16–19], which gives clues for designing partially oxidized Ag systems.

Furthermore, the mechanism studies are still lack of efficient techniques. Surface-enhanced Raman spectroscopy (SERS) is a powerful and non-destructive fingerprint spectroscopy, which can give the information in the low-frequency region without the influence of water [20]. SERS is also a perfect technique for detecting trace surface reaction intermediate species during CO_2 electroreduction *in situ* [7,8]. Ag has high SERS activity, and therefore Ag-based catalysts have the potential to provide SERS substrates to investigate the mechanisms of CO_2 electroreduction.

Herein, we used freshly prepared one-dimensional Ag nanowires (NWs) to improve the ethanol FE to as high as 85% for CO_2 electroreduction and further explained the mechanisms by *operando* Raman spectroscopy combined with density functional theory (DFT) calculations. X-ray photoelectron spectroscopy (XPS) and cyclic voltammograms (CVs) studies found that such freshly prepared Ag NWs were partially oxidized. Such Ag NWs achieved an extremely high ethanol FE of 85% at −0.95 V *vs*. reversible hydrogen electrode (RHE). *Operando* electrochemical SERS (EC-SERS) found that the CO intermediate with the high coverage can steer the pathway towards ethanol during CO_2 electroreduction, which explained why such Ag NWs exhibited high ethanol selectivity. DFT calculations found that the C–C coupling reaction of *CHO and CO to *CHOCO intermediates were the most favorable pathway for the formation of C_2 products on the partially oxidized Ag NWs, which facilitated the ethanol formation. Experimental results, *operando* EC-SERS combined with DFT calculations, found the partially oxidized Ag NWs can greatly improve the ethanol selectivity for CO_2 electroreduction.

2 Experimental

Well-defined Ag NWs were synthesized by a one-pot aqueous-phase hydrothermal strategy. Firstly, in a standard synthesis, 334 mg PVP was dissolved in 25 mL ethylene glycol and subsequently heated in an oil bath at 180 °C for 5 min under the continuous stirring at 320 rpm to remove water. Secondly, 50 μL ethylene glycol solution containing 0.43 mol L^{-1} NaCl and 50 μL ethylene glycol solution containing 0.43 mol L^{-1} $AgNO_3$ were synchronously injected into the container. 25 min later, 10 mL ethylene glycol solution containing 0.12 mol L^{-1} $AgNO_3$ was added to the mixture at a rate of 100 μL per 15 s. After 20 min, the milky white product appeared in the solution. And then, the rest of ethylene glycol solution was put into the mixture within 1 min. After the full injection of $AgNO_3$, the mixture was stirred for 15 min again. Finally, the cooled Ag NWs were centrifuged at 8,000 rpm for 10 min to remove the upper solution. The sediment was washed at 4,000 rpm for 10 min with ultrapure water and anhydrous ethanol 3 times for further electrochemistry and spectroscopy studies. The synthesis of Ag nanoparticles (NPs) and other experimental details were shown in the supporting information.

3 Results and discussion

3.1 Characterizations

X-ray diffraction (XRD), the transmission electron microscope (TEM) and scanning electron microscope (SEM) were used to characterize the Ag NWs. SEM images show that such Ag NWs are about 80 nm wide and more than 10 micrometers long (Figure 1a, b), while Ag NPs are about 80 nm (Figure S1). The TEM image of Ag NWs clearly shows the width of around 80 nm (Figure 1c) and high-resolution TEM image clearly shows a lattice fringe of around 0.236 nm corresponded to (111) plane of Ag (Figure 1d). XRD found that (111), (200), (222) and (311) facets exist in Ag NWs, while the Ag NWs and Ag NPs have the same PDF number of 04-0783 (Figure S2).

3.2 The catalytic activity and selectivity of CO_2 electroreduction

We then systematically investigated the electrocatalytic behavior of the Ag NWs and Ag NPs for CO_2 electroreduction. We relied on cyclic voltammetry (CV) to investigate the catalytic activity of CO_2 electroreduction. The current densities are normalized by the electrochemical surface area (Figure S3). The current density of Ag NWs and Ag NPs in the CO_2-saturated 0.5 mol L^{-1} $KHCO_3$ solution exhibited higher catalytic activity than that in the Ar-saturated one, indicating enhanced CO_2 electroreduction in the CO_2-satu-

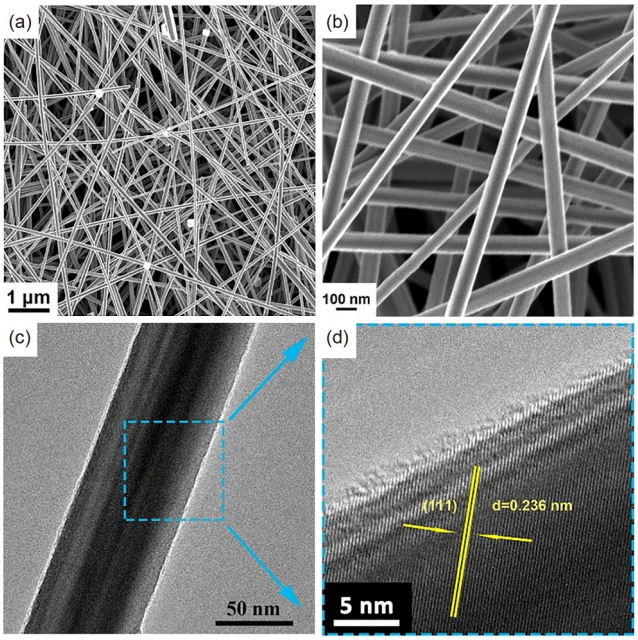

Figure 1 (a, b) SEM images of Ag NWs in different scales; (c) TEM image of Ag NWs; (d) high-resolution TEM image of Ag NWs (color online).

rated $KHCO_3$ solution because the carbonate concentration changes (Figure 2a, b and S1.6). The reversible peak at about −0.3–0 V was due to oxygen adsorption/desorption on the Ag surface of the Ag NWs and Ag NPs (Figure 2a, b) [21]. More detailed studies about the Ag electrooxidation were in Figure S5. Linear sweep voltammetry (LSV) curves were used to confirm the enhanced catalytic activity of Ag NWs and Ag NPs in the CO_2-saturated 0.5 mol L^{-1} $KHCO_3$ solution (Figure 2c, d). Therefore, the CO_2 electroreduction happened on both the Ag NWs and Ag NPs, and the Ag NWs exhibited higher CO_2 electroreduction activity than the Ag NPs (Figure 2c, d). By using a gas diffusion electrode (GDE), the current density can be greatly improved (Figure S6).

Besides the high catalytic activity, the selectivity of CO_2 electroreduction was more interesting and systematically investigated. Among all the products from CO_2 electroreduction, the liquid products were of most interest and quantified in the liquid phase using ^{1}H nuclear magnetic resonance (NMR) according to the literature [22]. The liquid products were quantified using dimethyl sulfoxide (DMSO) as a ^{1}H NMR internal standard according to the method described elsewhere (Figure S7) [22]. Based on the ^{1}H NMR and the current density, the FEs for different products were calculated for Ag NWs and Ag NPs at different potentials (Figure 3a, b). The main liquid CO_2 electroreduction products were ethanol for Ag NWs and formic acid for Ag NPs as detected by the ^{1}H NMR (Figures S8, S9). The ethanol FE and formic acid FE for Ag NWs and Ag NPs at different potentials are shown in Figure 3a, b, respectively. With the decrease of the potential, the ethanol selectivity first increases and then decreases, reaching the highest ethanol FE of around 85% for CO_2 electroreduction on Ag NWs at −0.95 V *vs*. RHE (Figure 3a). The Ag NWs also exhibited the high stability (Figure S10). However, the products for CO_2 electroreduction on Ag NPs is mainly HCOOH with a low FE in the aqueous solution (Figure 3b, Figure S9), while the main product is CO in the gas phase as detected by gas chromatograph (S1.10). What should be noted is that the ethanol selectivity for CO_2 electroreduction on Ag NWs is extremely high compared with the catalysts reported previously [7,23,24].

The question is why Ag NWs can efficiently convert CO_2 to ethanol while the Ag NPs cannot, and further studies are needed to make it clear. What interested us is the ethanol FE of such fresh Ag NWs decreases dramatically from 85% to 0% with the increase of the exposing time in the air on the first day to the 20th day (Figure 3c). In order to explain it, we detected the Ag/O atomic ratios of Ag NWs exposing different time in the air, and found that they decreased with the exposing time (Figure 3d). The XRD studies also found that the intensity of diffraction peaks decreased with the exposing time in the air, indicating the crystal structure changed with the oxidation in the air (Figure S2). The structures can greatly influence the catalytic properties. Ag NWs are covered mostly by (100) facets while Ag NPs covered mostly by (111) facets [25], which makes the Ag NPs easier to be oxidized than the Ag NWs [26]. Such different facets make the Ag–O and Ag–C bond adsorbed differently on Ag NWs and Ag NPs, which may finally change the ethanol selectivity [27].

XPS found that the Ag/O atomic ratios were 4.4 for Ag NWs and gradually decreased with the exposing time in the air, indicating that they were partially oxidized (Figure S11 and Table S2). Hereafter, we denoted such Ag NWs as partially oxidized Ag NWs. The Ag/O atomic ratios were about 1.9 for Ag NPs exposing for different time in the air (Figure 3d), indicating Ag NPs formed the equilibrium of oxygen-related layers immediately after exposing in the air. The oxidation of the Ag NPs' surface reached maximum immediately after exposing in the air. Therefore, the different facet structure can greatly influence the oxidation of Ag NWs and Ag NPs, which finally caused different ethanol selectivity. The CO_2 electroreduction on the Ag electrode before and after polishing was used to study the influence of the oxidation. The ethanol can be formed only after the Ag electrode is polished to remove the oxidized Ag (Figure S12).

3.3 *Operando* EC-SERS probing the intermediates

In order to make the mechanisms clear, *operando* EC-SERS was further used to investigate why such partially oxidized

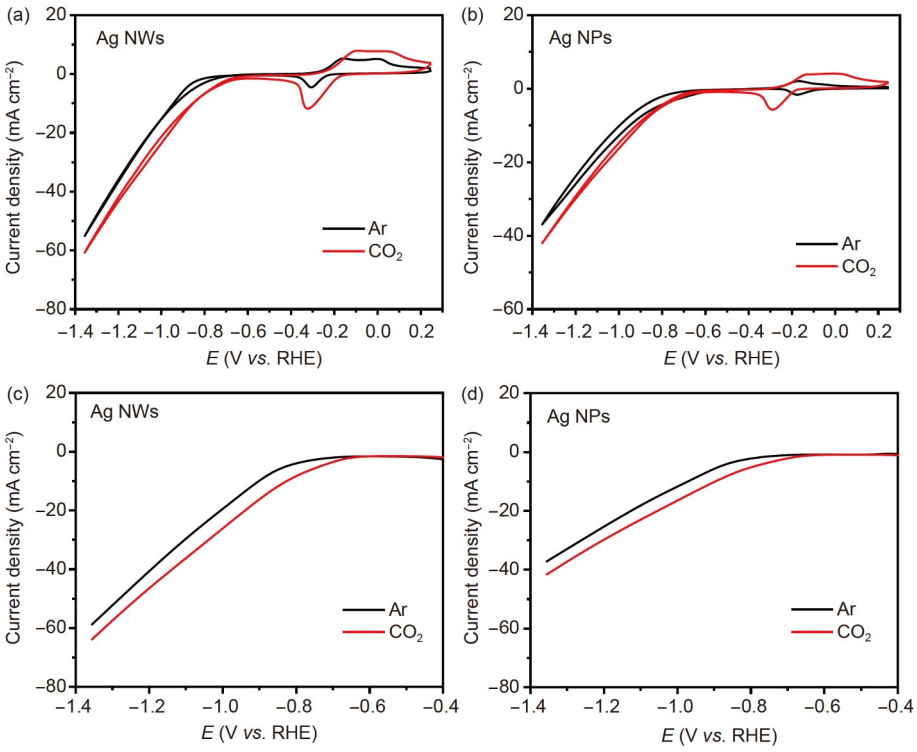

Figure 2 CV curves of Ag NWs (a) and Ag NPs (b) in a CO_2- or Ar-saturated 0.5 mol L^{-1} $KHCO_3$ solution; LSV curves of Ag NWs (c) and Ag NPs (d) in a CO_2- or Ar-saturated 0.5 mol L^{-1} $KHCO_3$ solution (color online).

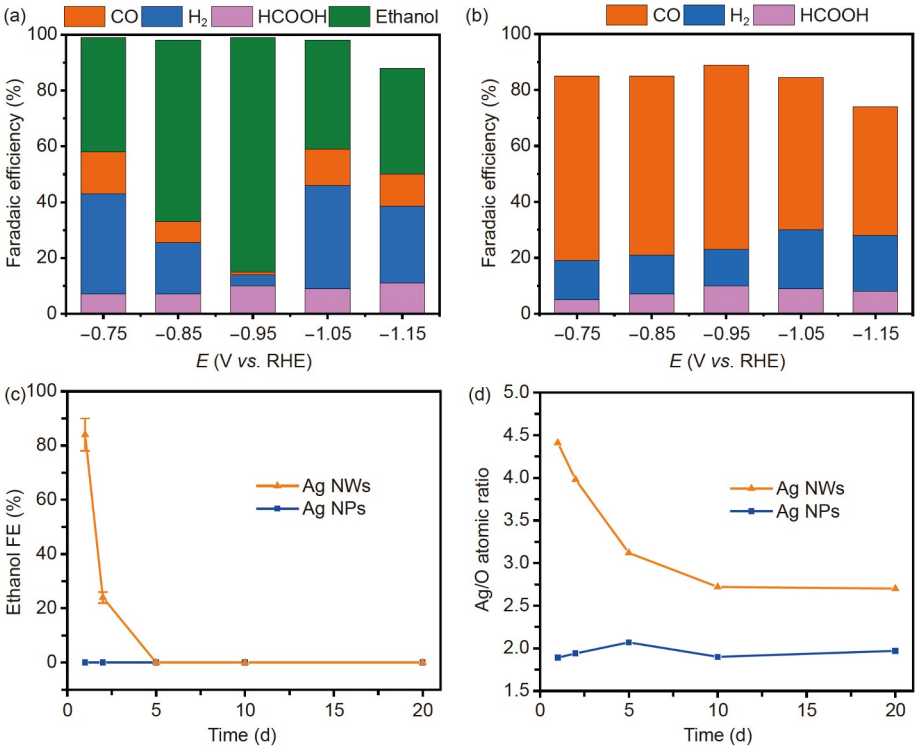

Figure 3 FE for ethanol and HCOOH products on (a) Ag NWs and (b) Ag NPs in 0.5 mol L^{-1} $KHCO_3$ at various applied potentials after reacting for 2 h; the dependence of ethanol FE (c) and Ag/O atomic ratios (d) for Ag NWs and Ag NPs on the exposing time in the air (color online).

Ag NWs were so efficient to convert CO_2 to ethanol. With the decrease of the potential, the observed strong peak at 2,101 cm^{-1} corresponded to the atop-adsorbed CO, while the peak at about 1,755 cm^{-1} was assigned to HCOOH adsorbed

on the partially oxidized Ag NWs at different potentials, and the corresponding Ag–C frequencies were also detected at 310 and 360 cm^{-1} (Figure 4) [7,15,28]. The strong CO SERS signal indicated a high surface coverage of *CO adsorbed on the partially oxidized Ag NWs, enhancing the C–C coupling and the formation of C_2 products [29,30]. Here, we achieved strong SERS signals of CO on the partially oxidized Ag NWs surface (Figure 4). However, no CO was detected on the Ag NPs, while only signals from carbonates (695 and 1,060 cm^{-1}), formic acid (1,755 cm^{-1}) [31], and the Ag–C (300 cm^{-1}) from the adsorption of carbonates were detected on Ag NPs during CO_2 electroreduction at different potentials (Figure S13). The carbonate was not detected on the Ag NWs because of the strong adsorption of CO. Therefore, the *operando* SERS has efficiently found the most important CO intermediate for forming ethanol, which explained why partially oxidized Ag NWs exhibited high ethanol selectivity.

Operando EC-SERS can also find the information of the oxygen adsorption/desorption on partially oxidized Ag NWs. In the low-frequency region, the reversible oxygen adsorbed on Ag NWs can be detected by SERS with a peak around 245 cm^{-1} (Figure 4). At the beginning, strong Ag–O peaks were observed at 0.45 V. Then, the Ag–O peak decreased gradually with the decrease of the potential and disappeared at −0.35 V, which was consistent with the CV curves in Figure 2a. It was more interesting that the CO peak can be detected together with the Ag–O peak, which meant that CO can be produced on the Ag surfaces with oxygen species adsorbed on. The CO peak increased gradually and reached the maximum at 0.05 V, at which the potential Ag–O peak still existed. When the Ag–O peaks disappeared, the CO-related SERS signal began to decrease, which indicated that the partially oxidized Ag surface can facilitate the CO adsorption. For the Ag NPs, no CO was detected, which made the adsorption of carbonates possible. Therefore, the high carbonate-related SERS signal was detected on the Ag NPs while no carbonate-related one was detected on the Ag NWs because of the strong adsorption of CO (Figure S13). Therefore, the partially oxidized Ag NWs can facilitate the formation and the adsorption of the CO, which greatly improves the ethanol selectivity.

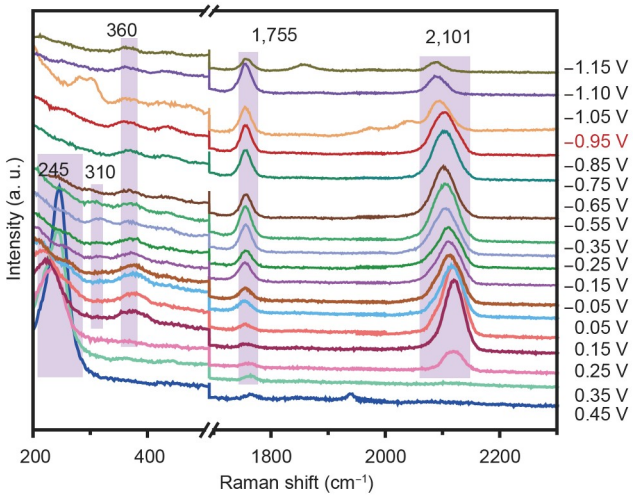

Figure 4 *Operando* EC-SERS spectra of CO_2 electroreduction on the surfaces of partially oxidized Ag NWs at different potentials in 0.5 mol L^{-1} $KHCO_3$ (color online).

3.4 DFT calculations to explain the mechanism

In order to further confirm the results from the EC-SERS, we performed DFT calculations for CO_2 reduction on Ag NWs and partially oxidized Ag NWs to gain insights into the reaction mechanisms. Recent mechanism studies have reached the consensus that the first process for the reduction of CO_2 to C_1 or C_2 products is the reduction of CO_2 to CO on Ag surfaces. Based on the previous studies [32–36], the following reaction mechanism of CO_2 reduction CO is considered as:

$$*CO_2+2H^++2e^-\rightarrow *COOH+H^++e^-\rightarrow *CO+H_2O$$

The calculated free energy diagrams of CO_2 reduction on Ag NWs are shown in Figure 5a while the adsorption configurations of intermediates are shown in Figure S14–16. The formation of carboxyl (*COOH) intermediates *via* proton coupling electron transfer process is the rate-determining step. Generally, CO is the final product for CO_2 electroreduction on Ag nanostructures due to the weak adsorption ability of CO on the Ag surface, and the adsorption energy of CO on Ag NWs is calculated to be −0.30 eV. The adsorption energy of CO on the surface of different Ag single crystals is shown in Table S3. Therefore, CO is the final product for CO_2 electroreduction on Ag through the *COOH pathway in the most cases [37].

However, in our case, Ag has already been partially oxidized on the Ag NWs (Figure 3d), which are totally different from the ordinary Ag structures. The adsorption energy of CO on the partially oxidized Ag NWs is calculated to be about −0.89 eV, which are close to the adsorption energy of CO adsorption on the Cu(111) surface (−0.98 eV), making the reaction activity of partially oxidized Ag NWs be similar with CO_2 reduction on the Cu(111) surface to C_2 product. Moreover, as shown in Figure 5a, the desorption of *CO is an endothermic reaction on the partially oxidized Ag NWs, which further suggests that the *CO can be further reduced on the partially oxidized Ag NWs. Furthermore, the high CO SERS signal detected in the *operando* Raman experiments in Figure 4 proved much higher CO coverage. When the CO coverage was further increased in the DFT calculation, the adsorption energy of CO on the partially oxidized Ag NWs was calculated to be −1.11 eV. The strong adsorption energy of the high coverage of CO greatly facilitates the formation of ethanol.

Figure 5 shows the detailed reaction mechanisms of CO_2

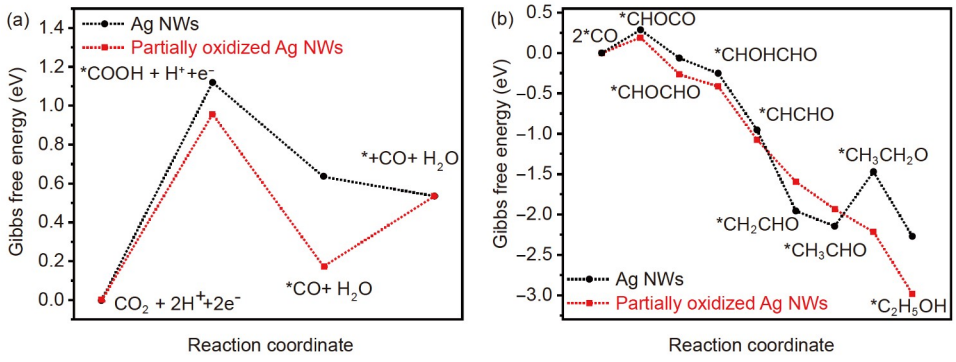

Figure 5 (a, b) The reaction energy diagram for the CO_2 reduction to ethanol at 0 V *vs*. RHE on the Ag NWs (black line) and partially oxidized Ag NWs (red line). All Gibbs free energies are provided relative to CO_2 and H_2 in the gas phase and a free metal surface (color online).

reduction to ethanol on the Ag NWs and the partially oxidized Ag NWs. The CO_2 reduction to *COOH intermediate is the rate-determinate step of the reaction, and the *CHOCO intermediate is the key step of CO reduction to C_2 production. Our calculation results show that the reduction energy of CO_2 to *COOH, and *COOH to CO on the partially oxidized Ag NWs is about 0.16 and 0.10 eV smaller than that on the Ag NWs, respectively. This suggests that the partially oxidized Ag NWs exhibit a higher reaction activity. Compared with the previous calculation results, the reaction energy of CO coupling with *CHO to *COCHO intermediate on the partially oxidized Ag NWs is smaller than that on the Cu surface [32]. The reaction intermediate of *CHOCO can be further reduced to ethanol through a series of exothermic elementary reaction (Figure 5b). Therefore, the DFT calculation explained our experimental results why such partially oxidized Ag NWs exhibit high ethanol selectivity for CO_2 electroreduction very well.

4 Conclusions

In conclusion, high ethanol FE was obtained on partially oxidized Ag NWs for CO_2 electroreduction, and *operando* EC-SERS combined with DFT calculations explained the mechanisms why partially oxidized Ag NWs exhibited so high ethanol selectivity. The ethanol FE can reach as high as 85% on the partially oxidized Ag NWs at −0.95 V *vs*. RHE. *Operando* EC-SERS found that the high coverage of CO can greatly facilitate the ethanol formation on the partially oxidized Ag NWs during CO_2 electroreduction. The DFT calculations result show that the adsorption energy of CO on the partially oxidized Ag NWs is higher than that on Cu, and the reaction free energy of CO coupling with *CHO to *COCHO intermediate on the partially oxidized Ag NWs is smaller than that on Cu surface, which explains the high ethanol selectivity very well. Therefore, experiment results, *operando* EC-SERS and DFT calculations together prove that such partially oxidized Ag NWs can provide high ethanol selectivity for CO_2 electroreduction. These results provide new ways for designing Ag-based electrocatalysts to improve the ethanol selectivity and mechanism studies.

Acknowledgements This work was supported by grants from the National Natural Science Foundation of China (22174165, 21925404, 22002036, and 21908253), the Natural Science Foundation of Guangdong Province (2019A1515011117), Guangdong Province Universities and Colleges Pearl River Scholar Funded Scheme (2017), and the Natural Science Foundation of Henan Province (202300410234).

Conflict of interest The authors declare no conflict of interest.

Supporting information The supporting information is available online at chem.scichina.com and link.springer.com/journal/11426. The supporting materials are published as submitted, without typesetting or editing. The responsibility for scientific accuracy and content remains entirely with the authors.

1 Gao S, Lin Y, Jiao X, Sun Y, Luo Q, Zhang W, Li D, Yang J, Xie Y. *Nature*, 2016, 529: 68–71
2 Liu C, Gong J, Gao Z, Xiao L, Wang G, Lu J, Zhuang L. *Sci China Chem*, 2021, 64: 1660–1678
3 Yang Y, Roh I, Louisia S, Chen C, Jin J, Yu S, Salmeron MB, Wang C, Yang P. *J Am Chem Soc*, 2022, 144: 8927–8931
4 Li S, Saranya G, Chen M, Zhu Y. *Sci China Chem*, 2020, 63: 722–730
5 Chen F, Shen K, Chen L, Li Y. *Sci China Chem*, 2022, 65: 1411–1419
6 Hoang TTH, Verma S, Ma S, Fister TT, Timoshenko J, Frenkel AI, Kenis PJA, Gewirth AA. *J Am Chem Soc*, 2018, 140: 5791–5797
7 Herzog A, Bergmann A, Jeon HS, Timoshenko J, Kühl S, Rettenmaier C, Lopez Luna M, Haase FT, Roldan Cuenya B. *Angew Chem Int Ed*, 2021, 60: 7426–7435
8 Chernyshova IV, Somasundaran P, Ponnurangam S. *Proc Natl Acad Sci USA*, 2018, 115: E9261–E9270
9 Zhang XG, Feng S, Zhan C, Wu DY, Zhao Y, Tian ZQ. *J Phys Chem Lett*, 2020, 11: 6593–6599
10 Hu F, Yang L, Jiang Y, Duan C, Wang X, Zeng L, Lv X, Duan D, Liu Q, Kong T, Jiang J, Long R, Xiong Y. *Angew Chem Int Ed*, 2021, 60: 26122–26127
11 Kong X, Wang C, Zheng H, Geng Z, Bao J, Zeng J. *Sci China Chem*, 2021, 64: 1096–1102
12 Hori Y, Wakebe H, Tsukamoto T, Koga O. *Surf Sci*, 1995, 335: 258–263
13 Raciti D, Braun T, Tackett BM, Xu H, Cruz M, Wiley BJ, Moffat TP. *ACS Catal*, 2021, 11: 11945–11959
14 Kong X, Zhao J, Ke J, Wang C, Li S, Si R, Liu B, Zeng J, Geng Z.

Nano Lett, 2022, 22: 3801–3808
15 Wang QY, Li YH, Zhao Y, Chen YY, Geng BJ, Ye RK, Liu Q, Liu XQ, Tong YX, Zhang YJ, Cheng J, Fang PP, Hu JQ, Li JF, Tian ZQ. *CCS Chem*, 2022, 4: 1–10
16 Favaro M, Xiao H, Cheng T, Goddard Iii WA, Yano J, Crumlin EJ. *Proc Natl Acad Sci USA*, 2017, 114: 6706–6711
17 Wang J, Tan HY, Zhu Y, Chu H, Chen HM. *Angew Chem Int Ed*, 2021, 60: 17254–17267
18 Xiao H, Goddard Iii WA, Cheng T, Liu Y. *Proc Natl Acad Sci USA*, 2017, 114: 6685–6688
19 Lin SC, Chang CC, Chiu SY, Pai HT, Liao TY, Hsu CS, Chiang WH, Tsai MK, Chen HM. *Nat Commun*, 2020, 11: 3525
20 Wang YH, Zheng S, Yang WM, Zhou RY, He QF, Radjenovic P, Dong JC, Li S, Zheng J, Yang ZL, Attard G, Pan F, Tian ZQ, Li JF. *Nature*, 2021, 600: 81–85
21 Savinova ER, Kraft P, Pettinger B, Doblhofer K. *J Electroanal Chem*, 1997, 430: 47–56
22 Rosen J, Hutchings GS, Lu Q, Rivera S, Zhou Y, Vlachos DG, Jiao F. *ACS Catal*, 2015, 5: 4293–4299
23 Yang B, Liu K, Li HJW, Liu C, Fu J, Li H, Huang JE, Ou P, Alkayyali T, Cai C, Duan Y, Liu H, An P, Zhang N, Li W, Qiu X, Jia C, Hu J, Chai L, Lin Z, Gao Y, Miyauchi M, Cortés E, Maier SA, Liu M. *J Am Chem Soc*, 2022, 144: 3039–3049
24 Zhang W, Huang C, Xiao Q, Yu L, Shuai L, An P, Zhang J, Qiu M, Ren Z, Yu Y. *J Am Chem Soc*, 2020, 142: 11417–11427
25 Xu H, Wiley BJ. *Chem Mater*, 2021, 33: 8301–8311
26 Li L, Yang JC. *Mater at High Temp*, 2003, 20: 601–606
27 Christopher P, Linic S. *J Am Chem Soc*, 2008, 130: 11264–11265
28 Gao J, Zhang H, Guo X, Luo J, Zakeeruddin SM, Ren D, Grätzel M. *J Am Chem Soc*, 2019, 141: 18704–18714
29 Verdaguer-Casadevall A, Li CW, Johansson TP, Scott SB, McKeown JT, Kumar M, Stephens IEL, Kanan MW, Chorkendorff I. *J Am Chem Soc*, 2015, 137: 9808–9811
30 Iyengar P, Kolb MJ, Pankhurst JR, Calle-Vallejo F, Buonsanti R. *ACS Catal*, 2021, 11: 4456–4463
31 Koper MTM, van Santen RA, Wasileski SA, Weaver MJ. *J Chem Phys*, 2000, 113: 4392–4407
32 Garza AJ, Bell AT, Head-Gordon M. *ACS Catal*, 2018, 8: 1490–1499
33 Yoo JS, Christensen R, Vegge T, Nørskov JK, Studt F. *ChemSusChem*, 2016, 9: 358–363
34 Kortlever R, Shen J, Schouten KJP, Calle-Vallejo F, Koper MTM. *J Phys Chem Lett*, 2015, 6: 4073–4082
35 Wang Z, Fongarland P, Lu G, Essayem N. *J Catal*, 2014, 318: 108–118
36 Hansen HA, Varley JB, Peterson AA, Nørskov JK. *J Phys Chem Lett*, 2013, 4: 388–392
37 Kuhl KP, Hatsukade T, Cave ER, Abram DN, Kibsgaard J, Jaramillo TF. *J Am Chem Soc*, 2014, 136: 14107–14113